Magnetic behavior of the $BaFe_{4-2x}Sn_{2+x}Co_xO_{11}$ system: From cluster glass to *kagomé* phase

B. Martínez and F. Sandiumenge
Institut de Cìencia de Materials de Barcelona, Consejo Superior de Investigaciones Científicas, Campus U.A.B., Bellaterra 08193, Spain

I. Golosovski
Petersburg Institute of Nuclear Physics, RA 188350 Gatchina, PNPI, Russia

S. Galí
Departament de Cristal·lografia, Universidad de Barcelona Martí i Franqués S/N, Barcelona 08028, Spain

A. Labarta
Departamento de Física Fundamental, Universidad de Barcelona Diagonal 647, Barcelona 08028, Spain

X. Obradors
Institut de Cìencia de Materials de Barcelona,, Consejo Superior de Investigaciones Científicas, Campus U.A.B., Bellaterra 08193, Spain
(Received 18 June 1993)

The cationic distribution of the solid solution $BaFe_{4-2x}Sn_{2+x}Co_xO_{11}$ ($0 \le x \le 2$) has been determined by using combined neutron and x-ray diffraction. A very strong cation site selectivity has been found: Sn atoms do not enter $4f(\frac{1}{2})$ sites at all, but this site is occupied by both Fe and Co atoms. On the other hand Sn atoms exhibit a strong preference for the 4*e* sites where Co atoms do not enter in any case. 6*g* sites are occupied by the three cations without any preference. No long-range magnetic ordering has been detected in any of the samples, but short-range three-dimensional ferrimagnetic ordering occurs below a temperature T_N that decreases as x increases. Below T_N down to T_F, the system is composed of a set of ferrimagnetic clusters of finite size. A second magnetic transition to a spin-glass-like phase is observed in all the samples at T_F, and this transition is attributed to the intrinsic frustration of the 6*g* sites arranged in a *kagomé* lattice.

I. INTRODUCTION

Hexagonal ferrites are a large family of hexagonal or rhombohedral ferrimagnetic oxides which have interesting applications as permanent magnets, microwave device materials, and magnetic and magneto-optical recording media.[1] Among these compounds, the most largely studied is the *M*-type barium ferrite $BaFe_{12}O_{19}$ (Ref. 2) due to its technological interest as a material suitable for high-density recording media.[3] Many efforts have been devoted to tailor its magnetic properties to fit better the technical requirements in each application. In this sense different doping schemes have been adopted for the partial substitution of Fe^{3+} ions[2,4] to reduce its high intrinsic magnetocrystalline anisotropy.[2] Besides the above-mentioned technological interest, recent studies have also shown interesting complex magnetic behaviors related to cation site selectivity, reflecting a complex interplay between ferrimagnetism and spin-glass (SG) ordering depending on the dilution rate.[5] The crystal structure of the *M*-type compounds (SG $P6_3/mmc$) can be described as the superposition of two structural blocks, namely, the *R* block with composition $(BaFe_6O_{11})^{2-}$ and the *S* block with composition $(Fe_6O_8)^{2+}$,[2] and each of these structural blocks may have interesting properties separately.

The first *R*-type hexagonal ferrite was synthesized by Haberey and Velicesu,[6] and charge neutrality was achieved by substituting trivalent iron with a tetravalent ion. The *R*-block structure is described in the $P6_3/mmc$ space group with $Z=2$ and is made up of three *c*-stacked oxygen layers, the middle one with composition BaO_3 and the other two with composition O_4. One oxygen anion is substituted by a cation in the BaO_3 layer, while other cations are distributed within two octahedral and two tetrahedral sites sharing a face in a mirror plane at the level of the BaO_3 layer.[7] The content of the unit cell of the *R* phase is described by a RR^* sequence where the asterisk denotes a 180° rotation around the *c* axis, plus $c/2$ translation.

Because of the multisublattice structure of hexagonal ferrites, competing exchange interactions among magnetic ions lead to a wide variety of magnetic orderings, such as local random spin canting, spin glass and reentrant spin glass, quasi-two-dimensional (2D) strongly frustrated behavior, etc.,[5,8–10] when some amount of Fe atoms is substituted with other atoms.

On the other hand, *R*-type hexagonal ferrites also have the intrinsic geometrically frustrated *kagomé lattice* (6*g* sites) that has been the subject of great interest due to its very special magnetic properties.[9,11] The *kagomé* lattice is made up of a network of corner-sharing triangles. The combination of antiferromagnetic interactions and a network of such geometrical units that frustrate the formation of a collinear ordered state leads to the appearance

of an intrinsic magnetic frustration that may exhibit very unusual behavior at low temperatures.[11]

In this paper we present the structural and magnetic characterization of the $Co^{2+}+Sn^{4+}$ doping scheme in the R-type $BaFe_{4-2x}Sn_{2+x}Co_xO_{11}$ hexagonal ferrite ($0 \leq x \leq 2$). No long-range ordering exists even in the sample with $x=0$ where the appearance of ferrimagnetic clusters is detected at room temperature. This short-range ferrimagnetic ordering temperature decreases linearly as the doping rate increases and disappears for $x=1.8$. Another peak that appears in the magnetic susceptibility in the low-temperature range through the whole range of compositions has been identified as the spin-glass ordering temperature generated by the intrinsic frustration of the *kagomé* lattice.

II. EXPERIMENTAL DETAILS

The samples were prepared by a solid-state reaction of mixtures of $BaCO_3$, SnO_2, Co_3O_4, and Fe_2O_3 (Merck pro-analysis) in the appropriate proportions to give $BaFe_{4-2x}Sn_{2+x}Co_xO_{11}$, $x=0$, 0.3, 0.6, 0.9. 1.2, 1.5, 1.8, and 2. The starting powders were homogenized in agate mortars, placed in platinum crucibles, and heated at 1300 °C for 1 week. During the process, the partial products were also homogenized and the extent of the reaction was checked by x-ray diffraction.

For the structural investigation, two sets of experiments were performed. First, x-ray diffractograms were recorded at room temperature on a Siemens D-500 automatic powder diffractometer equipped with a Cu $K\alpha$ source (wavelength 1.542 Å) in the angular range $10° < 2\theta < 100°$ with step width 0.05° and time per step 15 sec. Second, neutron-diffraction data were collected at room temperature in a multicounter neutron diffractometer at the Nuclear Physics Institute in Gatchina, in the angular range $0° < 2\theta < 100°$ (wavelength 1.63 Å) with step width 0.1° (2θ). The total measuring time was about 15 h per spectrum. In addition, the sample with $x=1.2$ was measured also at 4, 30, and 100 K.

Both dc and ac magnetic measurements were performed in the different samples of the series. dc magnetic measurements were carried out by using a Quantum Design superconducting quantum interference device (SQUID) magnetometer equipped with second-order gradiometer pickup coils in the temperature range from 4.2 to 800 K and applied magnetic fields ranging from 0 to 55 kOe. A Lakeshore ac susceptometer was used for the ac measurements, from room temperature to 4.2 K, in the frequency range from 5 Hz to 1 kHz and ac exciting fields from 0.1 to 14 Oe.

III. RESULTS

A. Cation distribution

Because of the similarity of the atomic numbers Z of Co and Fe, x-ray diffraction cannot give a unique solution to the distribution of the Co, Sn, and Fe species among the three different crystallographic sites of the R-like structure, namely, 4*e*, $4f(\frac{1}{2})$, and 6*g*. On the other hand, the Fermi lengths $b(\mathrm{Co})=2.50(3)\times10^{-12}$ cm, $b(\mathrm{Fe})=9.54(6)\times10^{-12}$ cm, and $b(\mathrm{Sn})=6.228(4)\times10^{-12}$ cm are different enough to permit the distinction between the species involved by using neutron diffraction.

In order to derive unequivocally the cation distribution in $BaFe_{4-2x}Sn_{2+x}Co_xO_{11}$ ($0 \leq x \leq 2$), in the present study we have taken advantage of both x-ray and neutron diffraction. A high preference of Sn atoms for occupying the face-sharing octahedral sites (4*e* sites, site number 2 in Fig. 1) was evident at the first stages of the x-ray refinement of the samples. The final results for the Sn location were subsequently used in the neutron refinements. The final results can then be used to construct the following system of nine equations with nine unknowns for each composition:

$$\begin{aligned} &p_j(\mathrm{Fe})Z(\mathrm{Fe})+p_j(\mathrm{Co})Z(\mathrm{Co})+p_j(\mathrm{Sn})Z(\mathrm{Sn})=\langle Z\rangle_j\ , \\ &p_j(\mathrm{Fe})b(\mathrm{Fe})+p_j(\mathrm{Co})b(\mathrm{Co})+p_j(\mathrm{Sn})Z(\mathrm{Sn})=\langle b\rangle_j\ , \\ &p_j(\mathrm{Fe})+p_j(\mathrm{Co})+p_j(\mathrm{Sn})=1\ , \end{aligned} \tag{1}$$

where the p's are the site occupation factors of the indicated cation in the crystallographic site j [$j=4e$, $4f(\frac{1}{2})$, 6*g*], the $\langle Z\rangle$'s are the average number of electrons, and the $\langle b\rangle$'s are the average Fermi lengths in crystallographic sites j. In this method, the overall composition is not constrained to the nominal sample one. The deviations of the derived sample compositions

$$q \approx p[\mathrm{Co},4f(\tfrac{1}{2})]+2p(\mathrm{Co},4e)+3p(\mathrm{Co},6g)\ ,$$

obtained from the nominal ones, were distributed among the three different sites and used as a realistic estimate of the errors. These results are displayed in Fig. 2.

It is evident from Fig. 2 that a very strong occupational hierarchy of the cation distribution exists. In order to understand the effect of dilution, i.e., of increasing x, on the magnetic behavior, it is essential to get a picture of the relative strength of the exchange interactions between neighboring sites, that is, the relative contribution of each crystallographic site to the macroscopic behavior of the sample. Isalgué *et al.*[12] reported a study of the magnetoplumbitelike compound $BaFe_{12}O_{19}$, in which the R

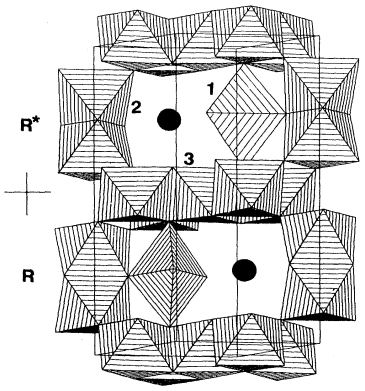

FIG. 1. STRUPLO drawing of the crystal structure of $BaFe_{4-2x}Sn_{2+x}Co_xO_{11}$ indicating the $4f(\frac{1}{2})$, 4*e*, and 6*g* sites (labeled 1, 2, and 3, respectively) and the Ba atom sites (black circles).

block is combined with the so-called spinel-like or *S* block to bring a . . . *SRS*R** . . . sequence. This study indicated that the face-sharing octahedra (4*e* sites) are actually the strongest superchange paths within the crystal structure, while for the edge-sharing octahedra lying at the contact between blocks (6*g* sites, site number 3 in Fig. 1), strongly competing interactions lower the stability of the spin arrangement. On the other hand, the magnetic cation located in the dipyramidal environment [$4f(\frac{1}{2})$ site, site number 1 in Fig. 1] was shown to provide a weak superexchange interaction with its nearest neighbors as a consequence of the fact that this cation is disordered between two pseudotetrahedral positions, thereby exhibiting an anomalously long cation to apical oxygen distance which diminishes drastically the atomic orbital overlap.

The structure of the *R*-like phase may be viewed (see Fig. 1) as a stacking of 2D layers of edge-sharing octahedra lying on the *R*-*R** interphases (6*g* sites) along the *c*-axis direction which define a *kagomé* lattice. These 2D slabs are connected one to each other through the face-sharing octahedra (4*e* sites) and the trigonal dipyramid [pseudotetrahedral $4f(\frac{1}{2})$ sites].

Figure 2 indicates a very strong cation site selectivity: Sn cations do not occupy the dipyramidal environment at all [Fig. 2(a)], and Co cations do not enter the face-sharing octahedra at all [Fig. 2(b)]. In the dipyramids, the rates of occupation by Co and Fe follow linear regimes and do not display a clear preference: A nearly random occupation can be envisaged. On the other hand, the nonincorporation of Sn^{4+} into these sites may be accounted for in terms of valency effects: Sn^{4+} tends to occupy the environments of higher coordination number, in agreement with experimental results obtained on x-ray single-crystal investigations. Figure 2(b) indicates a very strong affinity of Sn for the face-sharing octahedra (4*e* sites). From the crystallochemical point of view, the strong electrostatic repulsion between the two adjacent equivalent Sn^{4+} cations located at each side of the shared face induces an intense polyhedral distortion: The cation is shifted along the *c*-axis direction toward the neighboring empty octahedral sites, and the surface area of the shared face is reduced in order to screen the two neighboring Sn^{4+} cations. For $x=1.2$, the 4*e* sites are already almost fully occupied by Sn cations forming Sn_2O_9 groups. That means that for this composition, the strongest superexchange paths connecting the 2D *kagomé*-like slabs have been totally suppressed, thus enhancing the 2D character of the magnetic sublattice

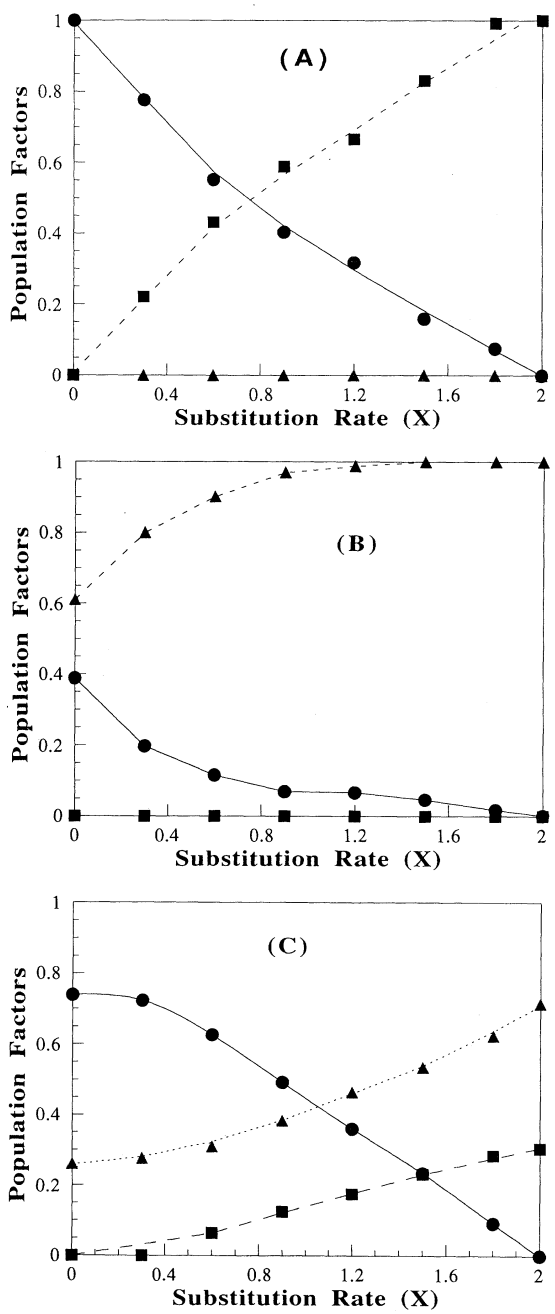

FIG. 2. Relative population of the three cations Fe (●), Sn (▲), and Co (■) in the (a) $4f\frac{1}{2}$, (b) 4*e*, and (c) 6*g* sites. The dimensions of the symbols are comparable to the estimated error. The lines are guides to the eye.

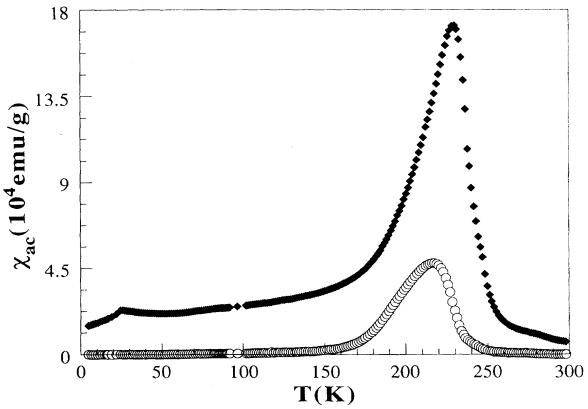

FIG. 3. Real (♦) and imaginary (○) parts of the ac susceptibility (χ_{ac}) of the sample having $x=0.6$ showing the appearance of two peaks at T_N (high-temperature range) and T_F (low-temperature range) ($H_{ac}\approx 5$ Oe, $\nu\approx 111$ Hz).

TABLE I. Dependence of the onset of irreversibility (T_N), magnetic frustration ($|\Theta|/T_F$), effective moment [$\mu_{eff}(\mu_B)$], and appearance of the *kagomé* phase (T_F) on the dilution x. The values for Θ and $\mu_{eff}(\mu_B)$ have been obtained from the Curie-Weiss law in the paramagnetic regime.

		T_F (K)				
X	T_N (K)	χ_{ac}	χ_{dc}	Θ (K)	$\lvert\Theta\rvert/T_F$	$\mu_{eff}(\mu_B)$
0	315	43	41			
0.3	265	32	30			
0.6	230	25.5	25			
0.9	165	20.3	20			
1.0	130	18	18	−95(5)	5.3(4)	5.4(1)
1.2	95	15.2	15	−81(5)	5.4(4)	5.2(1)
1.5	55	12.4	12	−66(5)	5.5(4)	4.9(1)
1.8	22	7.5	7.5	−45(4)	6.0(3)	4.8(1)
2.0	9	6	6	−44(4)	7.3(3)	4.4(1)

beyond $x=1.2$. Finally, the 6*g* edge-sharing octahedra forming the 2D slabs lying on the *R-R** interphase [Fig. 2(c)] display an almost linear substitution rate of Fe by Sn and Co. The slope of the Sn curve increases for x values larger than 1.2, in agreement with the fact that beyond this composition the 4*e* sites have already been filled by Sn. From Fig. 2(c) we can conclude that there exists no definite preference by either of the cations present for the 6*g* sites.

B. Magnetic measurements

The real χ' and imaginary χ'' parts of the ac susceptibility for the sample with $x=0.6$ are shown in Fig. 3. The real part χ' shows a sharp peak around $T_N \approx 225$ K and a small one around $T_F \approx 25$ K, while the imaginary χ'' goes through a maximum which corresponds to the inflection point of χ' below T_N and also shows a small anomaly at T_F. This is the general behavior observed in all the samples with composition $0 \leq x \leq 1.7$, but with the temperatures at which the peaks appear, T_N and T_F, decreasing almost linearly as x increases (see Table I). Samples having compositions with $x \geq 1.8$ do not show the high-temperature peak, but the one at T_F is still present (see Fig. 4). Above T_N the reciprocal of χ' shows a Curie-Weiss behavior with an effective moment intermediate between that of Fe^{3+} and Co^{2+} moments (see Fig. 5). To gain a deeper insight into the magnetic properties of the system, we have explored the dependence of both T_N and T_F on the frequency of the ac field obtaining that, while T_F is almost frequency independent, T_N shows a very remarkable dependence on the frequency of the excitation field. A good description of the frequency dependence of T_N is obtained by using a Vogel-Fulcher law[13]

$$\tau = \tau_0 \exp[E/k(T-T_0)] , \tag{2}$$

where T_0 can be viewed as a phenomelogic parameter which describes the intercluster interaction, with a characteristic microscopic relaxation time $\tau_0 \approx 10^{-12}$ sec, as can be seen in Fig. 6. This behavior is consistent with a cluster model in which the freezing phenomenon takes place in a set of superparamagnetic clusters. Each cluster has a probability to overcome the anisotropy energy barrier E, expressed in terms of a relaxation time τ, related to E by the Arrhenius law or the Vogel-Fulcher law.[13]

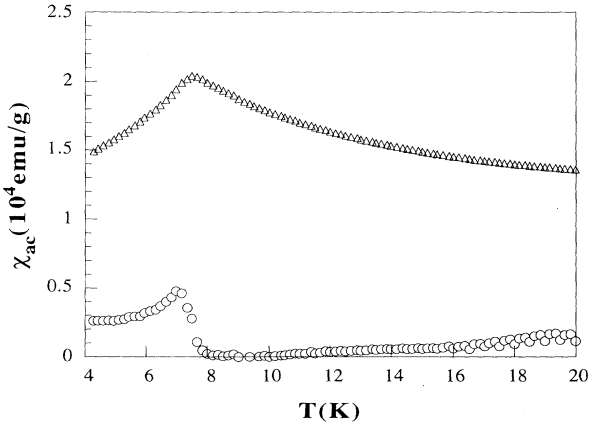

FIG. 4. Real (△) and imaginary (○) parts of the ac susceptibility (χ_{ac}) of the sample having $x=1.8$. Only the low-temperature peak at T_F remains in samples having $x \geq 1.8$ ($H_{ac} \approx 5$ Oe, $\nu \approx 111$ Hz).

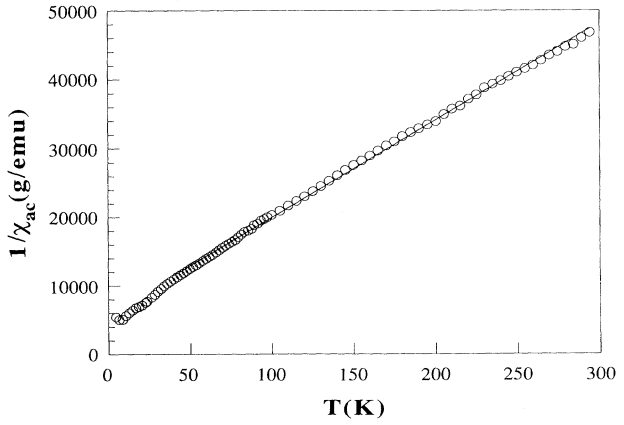

FIG. 5. Reciprocal of the ac susceptibility for the sample having $x=1.8$.

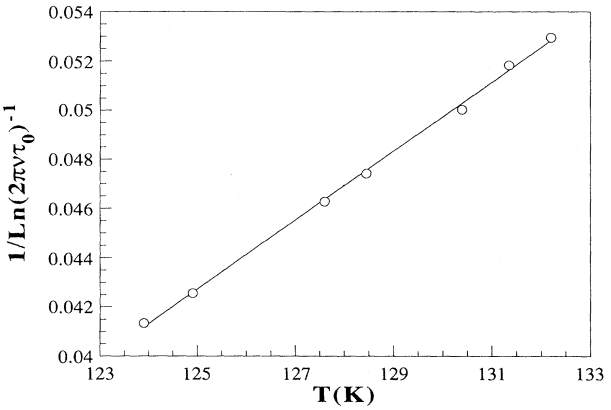

FIG. 6. Variation of the temperature of the cusp of the imaginary part of the ac susceptibility $\chi''_{ac}(T,\omega)$, with the frequency of the ac field in a Vogel-Fulcher plot for the sample having $x=1$.

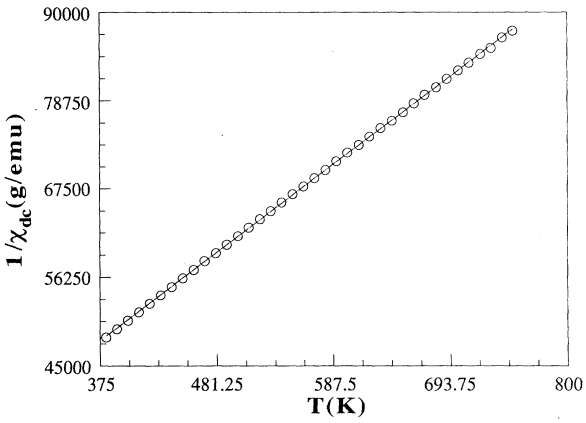

FIG. 8. Reciprocal of the dc susceptibility for the sample having $x \approx 1.2$ in the high-temperature range. The line represents a fit to the Curie-Weiss law.

On the other hand, in Fig. 7 we show the dc magnetic susceptibility after following the well-known zero-field-cooling–field-cooling (ZFC-FC) process for the sample with $x=0.6$. A very broad maximum appears in the high-temperature range with strong irreversibility between the ZFC and FC branches. The onset of irreversibility starts well above the cusp of the peak at approximately the same temperature T_N that the real part of the ac susceptibility has its maximum. Above this temperature both branches lie close together and the reciprocal of the susceptibility follows a Curie-Weiss law (see Fig. 8) with an effective moment matching that obtained from the ac measurements. The broadness of the peak and the fact that the irreversibility starts above the cusp of the peak give further clues to associate this peak with a thermally activated blocking process of ferrimagnetic clusters of different size. Another peak is also observed in the low-temperature range in the ZFC branch at T_F. It is worth mentioning that T_F is also clearly identified in the FC branch by a sudden change of the slope of the magnetic-susceptibility curve.

The same features are observed through all the samples having $x \leq 1.7$ with T_N and T_F decreasing linearly as the doping rate x increases (see Table I). For the samples having $x \geq 1.8$, the high-temperature peak is not present; nevertheless, it should be mentioned that some indications of it still persist in the ZFC branch of the magnetic susceptibility for the sample with $x \approx 1.8$ (see Fig. 9).

In order to clarify the nature of the magnetic ordering at T_N, we have studied the dc magnetic susceptibility as a function of the external applied field. A strong dependence of the susceptibility on the applied field is found (see Fig. 10), suggesting that no long-range magnetic ordering exist in any of the samples, in agreement with the neutron-powder-diffraction experiments on the $x=1.2$ sample which do not show magnetic-diffraction peaks within the limits of statistical accuracy. The magnetization curves do not show signs of magnetic saturation even at fields up to 55 kOe at any temperature, thus pointing

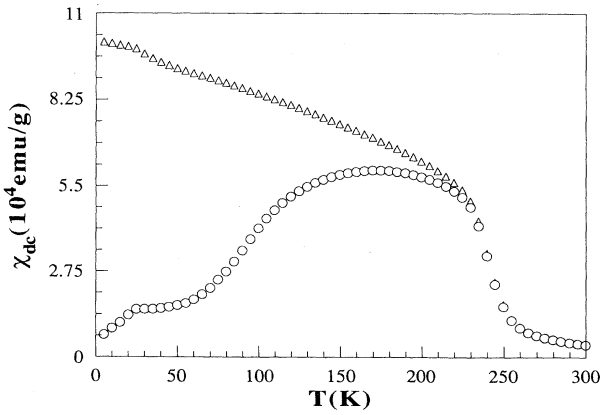

FIG. 7. ZFC (○) and FC (△) branches of the dc susceptibility for the sample having $x=0.6$, making evident the existence of strong irreversibility. The ZFC branch also shows a very broad peak starting at T_N and a small one at T_F.

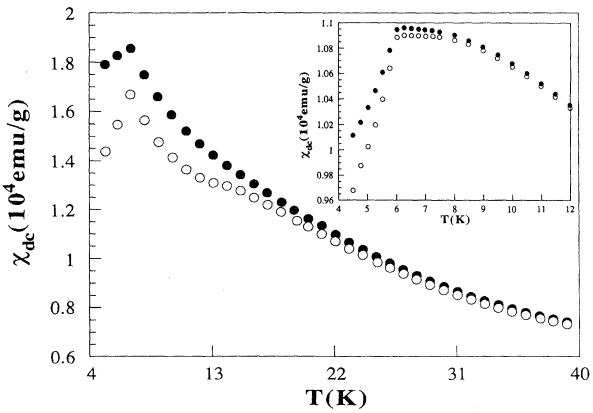

FIG. 9. Detail of the low-temperature range of the dc susceptibility after following a ZFC- (○) FC (●) process for the samples having $x \approx 1.8$ and $x \approx 2$ (inset).

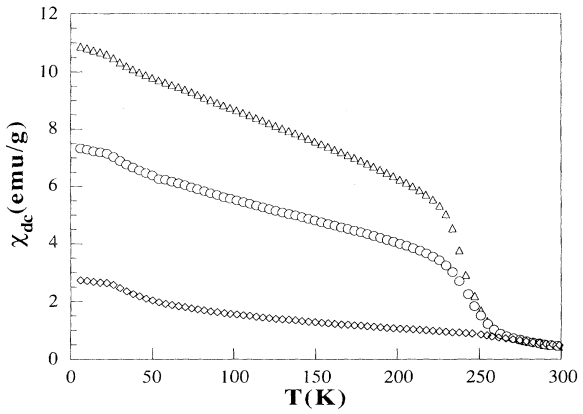

FIG. 10. Dependence of the dc susceptibility on the external applied field for the sample with $x=0.6$. 50 Oe, (△), 100 Oe (○), and 1000 Oe (◇).

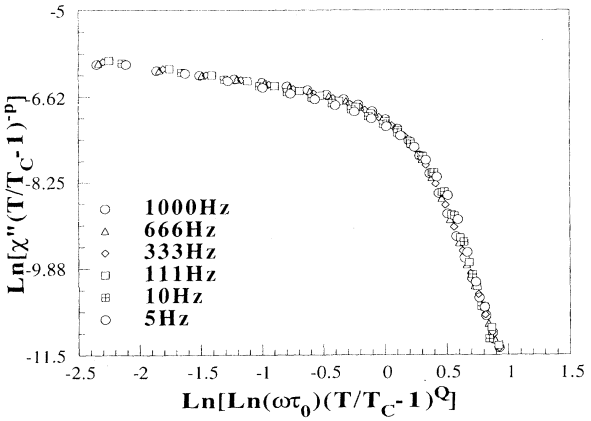

FIG. 11. Activated dynamic scaling of $\chi''_{ac}(T,\omega)$ data according to Eq. (3) corresponding to the sample with $x=1$.

out the existence of a noncollinear magnetic structure that is progressively oriented in the direction of the external applied field.

IV. DISCUSSION

Let us start the discussion of the results by addressing the problem of the dynamical behavior of the system. As we have commented above, the high-temperature peak shows a remarkable dependence on the frequency of the ac field as well as strong irreversibility, features that are both associated with the spin-glass behavior. There are basically two different interpretations of the spin-glass freezing phenomenon. One assumes the existence of a true equilibrium phase transition and is commonly accepted for canonical spin glasses, while in the other, the so-called cluster model, the spin glass is considered as a set of superparamagnetic clusters. In the latter case the freezing phenomenon is taken into account through the probability of each cluster to overcome the anisotropy energy barrier E, expressed in terms of a relaxation time τ, related to E by the Arrhenius or the Vogel-Fulcher laws.[13] We have studied the dynamic behavior of the high-temperature peak by analyzing the imaginary part of the ac susceptibility, $\chi''(T,\omega)$, using dynamic scaling theory.[14,15]

Activated dynamics reflects the presence of an effective free-energy barrier ΔE for the relaxation processes which scales as $\Delta E \approx \xi^{\theta}$ with the relaxation time given by $\tau \approx \tau_0 \exp[\Delta E/k_B T]$ or, what is equivalent, $\ln(\tau/\tau_0) \approx \xi^{\theta} \approx (T-T_C)^{-\nu\theta}$. In this framework the corresponding scaling relation may be written as

$$\chi''(T,\omega) = t^{P} G[-t^{Q}\ln(\omega\tau_0)] , \tag{3}$$

where P and Q are critical exponents, $t=(T-T_C)/T_C$ is the reduced temperature, and G is a universal scaling function. We have analyzed our $\chi''(T,\omega)$ data by using Eq. (3), obtaining a very good collapsing of the experimental data to a single curve (see Fig. 11) with the following set of parameters: $T_C \approx 125.5\pm0.5$ K, $P \approx 1.4\pm0.2$, $Q \approx 0.45\pm0.1$, and the value of τ_0 ($\approx 10^{-12}$ sec) obtained from the Vogel-Fulcher plot (Fig. 6). This set of critical exponents has been obtained by using the data corresponding to the $x \approx 1$ sample, but similar values, within the experimental error, are obtained for the rest of the samples having $x \leq 1.7$.

At this point it should be mentioned that a different set of critical exponents was reported in a preliminary paper,[16] but in this case the sample was composed of small single crystals (up to 1 mm) with an average value of the stoichiometric coefficient of $x \approx 1.1$, but with a dispersion of compositions ($0.9 \leq x \leq 1.3$). As can be appreciated in Fig. 4, the temperature T_N clearly depends on x, and so the results obtained in Ref. 16 may be affected by this dispersion of compositions or, what is the same, the dispersion of T_N. Thus the results of the scaling analysis reported in Ref. 16 may not be accurate.

With regard to the values of the exponents P and Q, it should be mentioned that they are in very good agreement with those previously reported by Geschwind *et al.*[17] in $Cd_{1-x}Mn_xTe$, $P=Q=0.65\pm0.1$, when properly taking into account the fact that $P(\chi'')=P(\Delta\chi')+Q$, applying the so-called "$\pi/2$ rule",[14] and also very similar to the set reported by Norblad, Lundgren, and Svedlingh[18] ($P=0.9\pm0.2$ and $Q=0.55\pm0.1$) in $Fe_{0.5}Mn_{0.5}TiO_2$. Nevertheless, they are completely different from the set found by Malozemoff and Pytte[15] in $Eu_{0.4}Sr_{0.6}S$ ($P=3\pm1$, $Q=0.65\pm0.15$) and by Zhou *et al.*[14] in $Cd_{0.7}Mn_{0.3}Te$ and $Hg_{0.7}Mn_{0.3}Te$ ($3.65 \leq P \leq 4.2$, $0.8 \leq Q \leq 1.2$). The nonuniversality of the P and Q exponents may indicate significant differences between the dynamic behavior of each system and hence that different relaxation processes take place.

We have also analyzed our data from the point of view of the existence of a true phase transition at T_N, but in contrast with the activated dynamic scaling, power-law scaling does not yield any acceptable results. Thus the image of a system composed of finite-size ferrimagnetic clusters whose dynamics is governed by free-energy barriers, and hence thermally activated, gets further confidence.

On the other hand, dc magnetic-susceptibility measure-

ments also point to a blocking process of ferrimagnetic clusters of different size, since its dependence on temperature (the broadness of the peak and the face that the irreversibility starts above the cusp of the peak) and field (strong dependence on the applied field) shows features usually taken as the fingerprints of the lack of long-range magnetic ordering.

dc magnetic measurements also show that all the samples having $x \geq 1$ follow a Curie-Weiss law above T_N with an effective moment between Fe^{3+}-Co^{2+} (see Table I). Nevertheless, it is worth pointing out that in order to obtain the correct value for the magnetic moment above T_N, it is necessary to go to very high temperatures (500–800 K). This fact makes evident the existence of very strong magnetic correlations in the system. For samples having $x \leq 0.9$, these magnetic correlations are so strong that even at 800 K the system is not in the true paramagnetic state and the values obtained for the magnetic moment and the extrapolated Curie temperature correspond to an effective value of the cluster system. The extrapolated Curie temperature Θ is negative, and its absolute value increases with x, indicating that antiferromagnetic interactions do exist in this family of compounds.

In order to gain a deeper insight into the magnetic behavior of the system, it is interesting to compare the intensity of the magnetic interactions between the moments located in the three different magnetic sublattices, namely, $4f(\frac{1}{2})$, 4*e*, and 6*g* (sites 1, 2, and 3, respectively, in Fig. 1). From Ref. 12 it turns out that the hierarchy of the magnetic interactions between the three magnetic sublattices is as follows: $J_{23} > J_{12} > J_{22} > J_{33} > J_{13} > J_{11} = 0$, being antiferromagnetic in all the cases and the first three clearly bigger than the rest. Having in mind this relation between the magnetic interactions, it is evident that the main path for magnetic interactions between two consecutive 6*g* layers is through the bottlenecklike structure composed of two 4*e* sites, since the interaction through the $4f(\frac{1}{2})$ sites, measured by J_{13}, is very small because of the fact that this cation is disordered between two pseudotetrahedral positions, thereby exhibiting an anomalous long cation to apical oxygen distance which diminishes drastically the atomic orbital overlap. Nevertheless, when the cation distribution of the three species Co, Fe, and Sm among the three magnetic sublattices is taken into account (see Fig. 2), it turns out that even in the sample with $x=0$ more than 60% of the 4*e* positions are occupied by Sn atoms, thus making the probability to find a path for the magnetic interactions through the 4*e* sites smaller than 0.16 and rapidly decreasing as x increases because of the strong preference of the Sn^{4+} ions for the 4*e* sites. Then the only remaining path for the magnetic interactions between the 6*g* layers is through the $4f(\frac{1}{2})$ sites, which are never occupied by Sn atoms, but that are the weakest of all the magnetic interactions in this structure as we have commented above.

Apart from its efficient destruction of the magnetic interaction through the 4*e* sites, the Sn atoms also play an important role in the macroscopic magnetic behavior of the system by increasing the degree of dilution of the magnetic moments in the 6*g* sites, thus decreasing drastically the probability to find a magnetic moment in the 6*g* sites as a nearest neighbor of a $4f(\frac{1}{2})$ magnetic moment. As a result of this, the appearance of long-range magnetic ordering is precluded and the size of the ferrimagnetic clusters decreases.

Having in mind these features of the cationic distribution, it is possible to explain the experimental result obtained in the high-temperature range. Long-range magnetic ordering is precluded in all of the samples of the series because of the very effective destruction of the paths of the magnetic interactions in the key points by the Sn atoms. Nevertheless, there exist clusters of finite size where 3D antiferromagnetic ordering is achieved. The formation of these clusters is reflected in the magnetic measurements by the appearance of a very broad peak as well as strong irreversibility in the dc magnetic susceptibility following a ZFC-FC process (see Fig. 7); a peak in the ac magnetic susceptibility is also observed at the same temperature as the onset of irreversibility (Fig. 3). The short-range character of this magnetic ordering is evidenced by the dependence of the magnetic susceptibility on the external applied field (see Fig. 10).

The study of the dynamic response of the system as a function of the frequency of the ac exciting field clearly points to a system composed of finite-size ferrimagnetic clusters whose dynamics is governed by a thermally activated process, thus confirming the short-range character of the magnetic ordering.

As the dilution of the magnetic species is increased through the coupled substitution of $2Fe^{3+}$ ions by $Co^{2+}+Sn^{4+}$ ions, the size of ferrimagnetic clusters decreases and this fact is reflected in a shift of the onset of irreversibility and the peak to lower temperatures that even disappears for the sample with $x=2$, where all the Fe atoms have been taken out, and only the low-temperature peak is observed. This shift of the onset of irreversibility to lower temperatures with increasing x gives further confidence to the role of the Sn atoms in controlling the size of the ferrimagnetic clusters.

We turn now to the low-temperature peak that appears at T_F through the whole series of samples of the solid solution $BaFe_{4-2x}Sn_{2+x}Co_xO_{11}$ ($0 \leq x \leq 2$). As we have commented in the paragraph devoted to the experimental results, the ac magnetic susceptibility of all the samples exhibits a peak in the real part and an anomaly in the imaginary part that do not show any dependence either on the ac frequency or on the intensity of the ac field. This dynamic behavior is very similar to that observed in the $SrCr_8Ga_4O_{19}$ compound[9] attributed to the strong intrinsic geometrical frustration of the 12*k* sites arranged in a *kagomé* lattice. Similarly, we attribute the peak at T_F in the present case to the spin-glass-like freezing phenomenon originated by the intrinsic frustration of the 6*g* sites that are also arranged in a *kagomé* lattice. The frustration inherent in the combination of antiferromagnetic interactions and a network of corner-sharing triangles can be easily appreciated by considering three antiferromagnetically coupled spins in a single triangle. Thus our samples present the two essential microscopic ingredients of a spin glass, namely, site disorder and bond frustration. The degree of magnetic frustration inferred

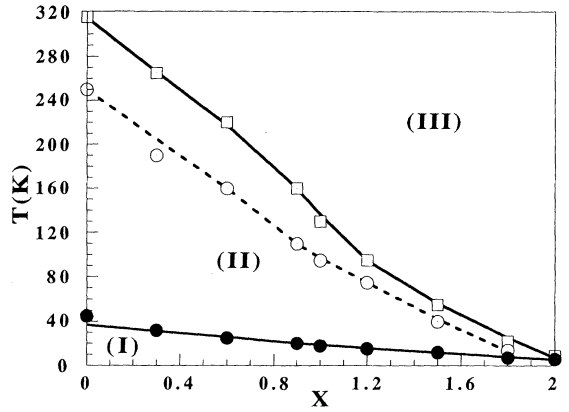

FIG. 12. Magnetic phase diagram of the solid solution $BaFe_{4-2x}Sn_{2+x}Co_xO_{11}$ $(0 \leq x \leq 2)$ as a function of the substitution rate x. (I) Spin-glass-like region (*kagomé* phase). (II) Ferrimagnetic clusters region [the onset of irreversibility (⊡) and the maximum of the ZFC peak (⊙) are indicated]. (III) Paramagnetic region. The lines are guides to the eye.

from the ratio $|\Theta|/T_F$ (see Table I) is much smaller than in the case of the $SrCr_8Ga_4O_{19}$ compound, but still reflects the existence of an intrinsic frustration due to the *kagomé* structure of the 6*g* sites. This frustration becomes more evident as the rest of the magnetic interactions are weakened by increasing the dilution of the magnetic moments and is reflected in the decrease of T_F and a small increase of the ratio $|\Theta|/T_F$ (see Table I) when the degree of dilution, x is increased. This increase of the influence of the intrinsic properties of the 6*g* *kagomé* layers over the magnetic properties of the whole structure may be understood by realizing that increasing the degree of dilution implies a more efficient destruction of the magnetic interaction between 6*g* layers since the probability to find a magnetic moment in the 6*g* layers as a nearest neighbor of a $4f(\frac{1}{2})$ magnetic moment decreases. Thus the influence of the intrinsic magnetic properties of 6*g* *kagomé* layers in the observed magnetic behavior of the system is enhanced through the dilution of the magnetic species by adding Sn.

At this point a magnetic phase diagram of the solid solution $BaFe_{4-2x}Sn_{2+x}Co_xO_{11}$ $(0 \leq x \leq 2)$ as a function of the degree of dilution (x) may be proposed (see Fig. 12). Below T_F the system exhibits spin-glass-like ordering, decreasing T_F as the degree of dilution increases. This spin-glass-like phase is generated as a result of the intrinsic geometrical frustration of the spins located in the 6*g* sites arranged in a *kagomé* lattice. Above T_F and until T_N, the system is composed of a set of ferrimagnetic clusters of different size, but no long-range magnetic ordering exists in any of the samples of the series $(0 \leq x \leq 2)$ as have been evidenced by neutron-powder-diffraction and magnetic measurements. T_N decreases as the degree of dilution increases. Above T_N all the samples exhibit paramagnetic behavior with an effective moment intermediate between Fe^{3+} and Co^{2+} moments.

V. CONCLUSIONS

We have determined the cationic distribution and studied the magnetic properties of the solid solution $BaFe_{4-2x}Sn_{2+x}Co_xO_{11}$ $(0 \leq x \leq 2)$ as a function of the degree of dilution x.

A very strong cation site selectivity has been detected: Sn atoms do not enter $4f(\frac{1}{2})$ sites at all; rather this site is occupied by Fe and Co atoms following a linear regime without clear preference. On the other hand, Sn atoms exhibit a strong preference for the 4*e* sites where Co atoms do not enter in any case. 6*g* sites are occupied by the three cations without any preference.

The strong preference of the Sn atoms for the 4*e* sites, which are the path for the strongest magnetic interaction between two consecutive 6*g* layers, makes impossible the appearance of long-range magnetic ordering in any of the samples of the series. Instead, short-range 3D ferrimagnetic ordering occurs below a temperature T_N that decreases as x increases following a quasilinear dependence. Below T_N down to T_F, the system is composed of a set of ferrimagnetic clusters of finite size, exhibiting strong irreversibility after a ZFC-FC process and a dynamic behavior typical of a system composed of finite-size ferrimagnetic clusters whose dynamics are governed by free-energy barriers and hence thermally activated. Strong magnetic correlations still remain well above T_N in all the samples, and in those rich in Fe $(x \leq 0.9)$ a pure paramagnetic behavior is not reached even at 750–800 K.

The existence of a second magnetic transition in all the samples of the series is indicated by a peak at T_F in both ac and dc magnetic susceptibility. This peak is associated with the appearance of spin-glass-like magnetic ordering in the samples generated by the intrinsic frustration of the 6*g* sites arranged in a *kagomé* lattice. The influence of the intrinsic magnetic properties of the 6*g* layers over that of the whole structure becomes more evident as the degree of magnetic dilution increases. Increasing the degree of dilution causes a more efficient destruction of the magnetic interaction between 6*g* layers, since the probability to find a magnetic moment in the 6*g* layers as a nearest neighbor of a $4f(\frac{1}{2})$ magnetic moment decreases.

ACKNOWLEDGMENT

This work has been supported by Spanish CICYT, Project No. MAT92-0263-C02-02.

[1]M. P. Sharrock, IEEE Trans. Magn. **MAG-25**, 4374 (1989).

[2]H. Kojima, in *Ferromagnetic Materials,* edited by E. P. Wolthfarth (North-Holland, Amsterdam, 1982), Vol. 3; J. Smit and H. P. J. Wijn, in *Ferrites* (Phylips Technical Library, Einhoven, 1960).

[3]S. Iwasaki, IEEE Trans. Magn. **MAG-20**, 654 (1984).

[4]O. Kubo, T. Ido, and H. Yokoyama; IEEE Trans. Magn. **MAG-18**, 1112 (1982); X. Batlle, X. Obradors, M. Pernet, M.

Vallet, M. V. Cabañas, J. Rodríguez, and J. Fontcuberta; J. Magn. Magn. Mater. **83**, 465 (1990); X. Batlle, X. Obradors, J. Rodríguez, M. Pernet, M. V. Cabañas, and M. Vallet, J. Appl. Phys. **70**, 1614 (1991).

[5]K. Iwauchi and Y. Ikeda, J. Magn. Magn. Mater. **59**, 73 (1986); G. M. Irwin and E. R. Sanford, Phys. Rev. B **44**, 4423 (1991).

[6]V. F. Haberey and M. Velicescu, Acta Crystallogr. B **30**, 1507 (1974).

[7]X. Obradors, A. Collomb, M. Pernet, D. Samaras, and J. C. Joubert, J. Solid State Chem. **56**, 171 (1981).

[8]A. Labarta, X. Batlle, B. Martínez, and X. Obradors, Phys. Rev. B **46**, 8994 (1992).

[9]B. Martínez, F. Sandiumenge, A. Rouco, A. Labarta, J. Rodríguez, M. Tovar, M. T. Causa, S. Galí, and X. Obradors, Phys. Rev. B **46**, 10 786 (1992).

[10]X. Obradors, A. Isalgué, A. Collomb, M. Pernet, J. A. Pereda, J. Tejada, and J. C. Joubert, J. Phys. C **19**, 6605 (1986); X. Obradors, A. Isalgué, A. Collomb, M. Pernet, J. Tejada, and J. C. Joubert, J. Phys. (Paris) Colloq. **46**, C6-339 (1985).

[11]A. P. Ramírez, G. P. Espinosa, and A. S. Cooper, Phys. Rev. Lett. **64**, 2070 (1990); Phys. Rev. B **45**, 2505 (1992); C. Broholm, G. Aeppli, G. P. Espinosa, and A. S. Cooper, Phys. Rev. Lett. **65**, 3173 (1990); J. Appl. Phys. **69**, 4968 (1991).

[12]A. Isalgué, A. Labarta, J. Tejada, and X. Obradors, Appl. Phys. A **39**, 221 (1986).

[13]J. L. Tholence, Solid State Commun. **35**, 113 (1980).

[14]Y. Zhou, C. Rigaux, A. Mycielsky, M. Menant, and N. Bontemps, Phys. Rev. B **40**, 8111 (1989); D. S. Fischer, J. Appl. Phys. **61**, 3672 (1987).

[15]A. P. Molozemoff and E. Pytte, Phys. Rev. B **34**, 6579 (1986).

[16]M. Martínez, F. Sandiumenge, S. Galí, X. Obradors, and R. Rodríguez-Clemente, Solid State Commun. **83**, 649 (1992).

[17]S. Geschwind, A. T. Ogielski, G. Devlin, and J. Hegarty, J. Appl. Phys. **63**, 3291 (1988).

[18]P. Nordblad, L. Lundgren, and P. Svedlingh, J. Phys. (Paris) Colloq. **49**, C8-1069 (1988).